the plant journal

SEB SOCIETY FOR EXPERIMENTAL BIOLOGY

The Plant Journal (2020) **103,** 1372–1385 doi: 10.1111/tpj.14806

Cell wall composition strongly influences mesophyll conductance in gymnosperms

Marc Carriquí[1,2,†,*], Miquel Nadal[1,†], María J. Clemente-Moreno[1], Jorge Gago[1], Eva Miedes[3,4] and Jaume Flexas[1]

[1]*Research Group in Plant Biology under Mediterranean Conditions, Universitat de les Illes Balears (UIB) – Agro-Environmental and Water Economics Institute (INAGEA), Palma, Illes Balears, 07122, Spain,*

[2]*School of Natural Sciences, University of Tasmania (UTAS), Bag 55, Hobart, Tasmania, 7001, Australia,*

[3]*Centro de Biotecnología y Genómica de Plantas, Universidad Politécnica de Madrid (UPM), Instituto Nacional de Investigación y Tecnología Agraria y Alimentaria (INIA), Campus Montegancedo UPM, Pozuelo de Alarcón, Madrid 28223, Spain, and*

[4]*Departamento de Biotecnología-Biología Vegetal, Escuela Técnica Superior de Ingeniería Agronómica, Alimentaria y de Biosistemas, Madrid 28040, Spain*

Received 23 March 2020; revised 22 April 2020; accepted 28 April 2020; published online 11 May 2020.
*For correspondence (e-mail mcarriqui@gmail.com).
†These authors equally contributed to this work.

SUMMARY

Cell wall thickness is widely recognized as one of the main determinants of mesophyll conductance to CO_2 (g_m). However, little is known about the components that regulate effective CO_2 diffusivity in the cell wall (i.e. the ratio between actual porosity and tortuosity, the other two biophysical diffusion properties of cell walls). The aim of this study was to assess, at the interspecific level, potential relationships between cell wall composition, cell wall thickness (T_{cw}) and g_m. Gymnosperms constitute an ideal group to deepen these relationships, as they present, on average, the thickest cell walls within spermatophytes. We characterized the foliar gas exchange, the morphoanatomical traits related with g_m, the leaf fraction constituted by cell walls and three main components of primary cell walls (hemicelluloses, cellulose and pectins) in seven gymnosperm species. We found that, although the relatively low g_m of gymnosperms was mainly determined by their elevated T_{cw}, g_m was also strongly correlated with cell wall composition, which presumably sets the final effective CO_2 diffusivity. The data presented here suggest that (i) differences in g_m are strongly correlated to the pectins to hemicelluloses and cellulose ratio in gymnosperms, and (ii) variations in cell wall composition may modify effective CO_2 diffusivity in the cell wall to compensate the negative impact of thickened walls. We speculate that higher relative pectin content allows higher g_m because pectins increase cell wall hydrophilicity and CO_2 molecules cross the wall dissolved in water.

Keywords: cell wall composition, cell wall thickness, mesophyll conductance, photosynthesis, leaf anatomy, cellulose, hemicellulose, pectin.

INTRODUCTION

Mesophyll conductance (g_m) is one of the three main limitations [together with stomatal conductance (g_s) and the biochemical capacity] to net CO_2 assimilation (A_N) (Cousins *et al.*, 2020; Lawson and Flexas, 2020). In the mesophyll, CO_2 molecules must diffuse through a gas-phase resistance, the intercellular air space path from the substomatal cavity to the cell wall surface, and several liquid-phase resistances, composed by the apoplast and the different cellular structures that separate the cell wall surface from the carboxylation site into the stroma (i.e. cell wall, plasma membrane, cytoplasm, chloroplast envelope and stroma; Evans *et al.*, 2009; Terashima *et al.*, 2011). The relevance of each resistance depends on structural (path lengths and surface areas of each trait) and biochemical determinants – suggested to be mostly aquaporins in cell membranes and carbonic anhydrases in the cytosol and chloroplast stroma (Flexas *et al.*, 2012; Flexas *et al.*, 2018; Gago *et al.*, 2020; Momayyezi *et al.*, 2020). The structural determinants, which set a maximum g_m, can change in response to specific environmental conditions (e.g. Tholen *et al.*, 2008; Morales *et al.*, 2014; Momayyezi and Guy, 2017), or during leaf ontogeny (Miyazawa and Terashima, 2001; Tosens *et al.*, 2012a), although are probably quite static in the

seconds to minutes range (Carriquí *et al.*, 2019a). On the other hand, the biochemical determinants can be regulated at all time scales (Bernacchi *et al.*, 2001; Yamori *et al.*, 2014). In addition, anatomical and biochemical determinants present a wide range of variation, partially explaining the differences in the photosynthetic capacity between species or even genotypes (Muir *et al.*, 2014; Carriquí *et al.*, 2015; Tosens *et al.*, 2016; Peguero-Pina *et al.*, 2017; Veromann-Jürgenson *et al.*, 2017; Carriquí *et al.*, 2019b; Gago *et al.*, 2019; Flexas and Carriquí, 2020). However, there are still uncertainties regarding the biophysical diffusion properties of the different components of the diffusion pathway. Such uncertainties may affect mesophyll cell walls, a key component of the CO_2 pathway that drives g_m in many species (Terashima *et al.*, 2011; Tosens *et al.*, 2016; Veromann-Jürgenson *et al.*, 2017; Ellsworth *et al.*, 2018; Gago *et al.*, 2019; Carriquí *et al.*, 2019b).

Cell wall resistance to CO_2 diffusion may depend on at least three physical wall properties (thickness, porosity and tortuosity) (Niinemets and Reichstein, 2003; Nobel, 2004; Evans *et al.*, 2009), although a direct effect of chemical interactions between cell wall components and diffusing CO_2 cannot be ruled out (Ellsworth *et al.*, 2018; Clemente-Moreno *et al.*, 2019). Cell wall thickness can be easily determined using transmission electron microscopy (TEM) images and has been assessed in species from all major land plant groups (Veromann-Jürgenson *et al.*, 2017; Gago *et al.*, 2019; Carriquí *et al.*, 2019b), revealing the existence of a strong exponential decay of g_m as T_{cw} increases (Onoda *et al.*, 2017; Ren *et al.*, 2019; Carriquí *et al.*, 2019b). For cell walls thinner than 0.4 μm, g_m values can range between 0.03 and 0.76 mol m^{-2} sec^{-1}. However, when T_{cw} >0.4 μm none of the reported correspondent g_m values were >0.12 mol m^{-2} sec^{-1} (Veromann-Jürgenson *et al.*, 2017; Onoda *et al.*, 2017; Ren *et al.*, 2019; Carriquí *et al.*, 2019b). Thus, while in the 0.1–0.4 μm range a small increase in T_{cw} has a large quantitative negative effect on g_m, with cell walls thicker than approximately 0.4 μm g_m values are always low, but not necessarily increasingly lower as the T_{cw} increases. This suggests that species with thicker cell walls might compensate this handicap by modifying other traits, including their cell wall effective diffusivity (=porosity/tortuosity), to achieve similar g_m values to other species irrespective of cell wall thickness. However, due to methodological limitations, there is little information available on the effective diffusivity of cell walls in land plants. Although there are no direct measurements of the effective CO_2 diffusivity in the cell wall, several authors have tried to estimate it. Nobel (2004) first postulated, based only on physicochemical estimations, that effective diffusivity would be approximately 0.3 m^3 m^{-3}, which implies that cell wall conductance is not small enough to constrain A_N. Then, Terashima *et al.* (2006), based on the variability of g_m between species for a given S_c/S, proposed a cell wall effective diffusivity value of ≤0.1 m^3 m^{-3}, implying that cell wall porosity and/or tortuosity would be a key determinant of g_m. Terashima *et al.* (2006) also noted, based on previous studies of cell wall permeability to H_2O on algae with >10 μm thick cell walls, that effective diffusivity might be inversely proportional to the thickness of the cell walls. Later, Evans *et al.* (2009) suggested that the effective diffusivity value could be 0.07 m^3 m^{-3} based on a simple model of the CO_2 pathway through pores from onion cell wall images from McCann *et al.* (1990). From then on, due to lack of accurate measurements of wall resistance to CO_2 diffusion, several authors have been using these published values in analytical models based on anatomical traits to estimate g_m. While some authors considered a constant effective diffusivity, some others adjusted it to be correlated with cell wall thickness following either a linear or an exponential decay function (Peguero-Pina *et al.*, 2012; Tosens *et al.*, 2012a,b; Tomás *et al.*, 2013; Tomás *et al.*, 2014; Carriquí *et al.*, 2015; Tosens *et al.*, 2016; Veromann-Jürgenson *et al.*, 2017; Xiao and Zhu, 2017; Han *et al.*, 2018). Such approaches based solely on assumptions can lead to an under- or overestimation of the cell wall role on g_m and thus A_N.

Cell wall composition remains an almost unexplored factor that could affect g_m through its effects on porosity and tortuosity. Primary cell walls are mainly composed of a relatively small number of basic components: microfibrils of cellulose and a matrix of hemicelluloses, pectins and structural proteins (Cosgrove, 2005; Sarkar *et al.*, 2009; Cosgrove and Jarvis, 2012). The structure, organization and interactions of microfibrils and the glycan matrix form a tangled web resulting in nanometric and micrometric pores that regulate the exchange of macromolecules, water and gases (Carpita *et al.*, 1979; Evans *et al.*, 2009). This cell wall assembly is regulated during cell elongation and differentiation (Rondeau-Mouro *et al.*, 2008; Cosgrove, 2016), is constantly remodelled and reconstructed (Sarkar *et al.*, 2009; Bellincampi *et al.*, 2014; Houston *et al.*, 2016) and is more complex than traditionally thought (Maron, 2019; Zhang *et al.*, 2019). The result is an intricate pathway that determines a pore size, which limits or hinders the crossing of molecules depending on its size and interaction with the wall components. CO_2 molecules can cross cell walls because they are several times smaller than pore diameter (Carpita *et al.*, 1979; Read and Bacic 1996; Evans *et al.*, 2009). Although cell wall porosity in higher plants is known to be regulated by cell wall composition, particularly by pectins in the primary cell walls (Baron-Epel *et al.*, 1988; Fleischer *et al.*, 1999; Rondeau-Mouro *et al.*, 2008), little information is available for its direct effect on CO_2 diffusion. Weraduwage *et al.* (2016) reported that the genetic manipulation of the pectin methyl esterification level, which modulates cell wall plasticity and plant growth,

affected the relationship between photosynthesis and plant growth. However, while this effect could potentially be explained by changes in the cell wall properties affecting CO_2 diffusion, g_m and T_{cw} were not determined in this study. Another indirect evidence was found by Gago *et al.* (2016), who reported significant interspecific associations between g_m and the main oligomers of the hemicelluloses and pectins (e.g. galactose, arabinose, mannose, xylose and gluconate), as well as with phenolic precursors related to cell walls, such as hydroxybenzoate, and γ-aminobutyric acid, the latter having been reported as a molecule with a potential signalling role for growth/cell wall rearrangement (Renault *et al.*, 2010). Altogether, evidence suggests a relationship between g_m functionality and cell wall dynamic metabolism (Gago *et al.*, 2016). Moreover, Ellsworth *et al.* (2018) deduced that cell wall effective diffusivity had a relevant effect on g_m from the differences in physiology and leaf anatomy observed in rice mutants lacking mixed-linkage glucan. Recently, Clemente-Moreno *et al.* (2019) showed that apoplastic metabolism and cell wall composition (pectin content and cell wall-related metabolites) in tobacco leaves changed in response to short-term abiotic stresses, in association with variations in mesophyll conductance to CO_2 diffusion. Finally, Roig-Oliver *et al.* (2020) suggested a role of cell wall composition modulated by acclimation to contrasting environmental conditions on photosynthesis and water relations in grapevines. However, a multispecies comparison of the potential effects of cell wall composition on g_m is lacking. In addition, the relationship between mesophyll cell wall composition and thickness remains unexplored.

Based on evidence, we hypothesize that cell wall composition could have a significant role on the existing differences in wall conductance to CO_2 between species acclimated to common environmental conditions. To test this hypothesis, we selected a group of seven gymnosperm species, as most of them have thick cell walls and present high interspecific T_{cw} variability (Peguero-Pina *et al.*, 2012; Veromann-Jürgenson *et al.*, 2017; Kuusk *et al.*, 2018), and to avoid extra sources of variation due to the probable differences in cell wall components between more distant plant groups (Sarkar *et al.*, 2009; Popper *et al.*, 2011). To test the hypothesis that g_m changes in parallel to cell wall composition, we estimated g_m and characterized both leaf morphoanatomy and cell wall composition in the seven gymnosperm species to explore for correlative evidence between g_m and cell wall thickness and composition in this land plant group. Specifically, we considered that the negative effect of increased T_{cw} on g_m found in gymnosperms would be compensated by at least one of the following two possibilities, (i) the implication of other components of the mesophyll CO_2 pathway, or (ii) interspecific differences in the effective diffusivity of CO_2 in the cell wall (i.e. the combined effect of cell wall porosity and tortuosity), not necessarily related to T_{cw}. In the present work, we focus on the second aspect.

RESULTS

Photosynthetic capacity and its physiological constraints

The gymnosperm species sampled here (i.e. *Chamaecyparis obtusa*, *Juniperus oxycedrus*, *Picea glauca*, *Sequoiadendron giganteum*, *Taxus baccata*, *Taxus cuspidata* and *Thuja plicata*) exhibited a narrow range of variation in their physiological performance (Table 1). Net assimilation (A_N) ranged two-fold from 4.3 ± 0.3 μmol m^{-2} sec^{-1} in *Chamaecyparis obtusa* to 9.2 ± 0.4 μmol m^{-2} sec^{-1} in *T. baccata*, whereas stomatal and mesophyll conductance estimated from chlorophyll fluorescence (g_s and g_{m_FLU}, respectively) varied about two- and three-fold, respectively. g_s ranged from 0.033 ± 0.004 in *C. obtusa* to 0.095 ± 0.013 mol m^{-2} sec^{-1} in *S. giganteum*, and g_{m_FLU} varied from 0.047 ± 0.015 in *J. oxycedrus* to 0.104 ± 0.025 mol m^{-2} sec^{-1} in *T. baccata*. A_N was linearly correlated with g_s ($r^2 = 0.69$, $P < 0.0001$) and g_{m_FLU} ($r^2 = 0.28$, $P < 0.05$) across species when also considering the gymnosperm species reported by Veromann-Jürgenson *et al.* (2017) (Figure 1a,b). In the case of the A_N-g_m relationship, the significance of the correlation is loosened by *Cupressus sempervirens*, which presents a higher $A_N \cdot g_m^{-1}$, and by *Chamaecyparis obtusa* and *Cycas revoluta*, which present a lower $A_N \cdot g_m^{-1}$ (Figure 1b). Diffusive limitations (the sum of stomatal and mesophyll conductance limitations) were the main factors constraining A_N (from 56% to 68%; Table S1).

Morphoanatomical determinants of mesophyll conductance

Leaf morphological and anatomical traits potentially involved in setting A_N and g_m varied among species (Table 2; Tables S2 and S3), but had values generally within the previously reported ranges for gymnosperms (Figure S1). High leaf dry mass per unit area (LMA) but also high leaf thickness (T_{leaf}) values lead to leaf density (D_{leaf}) ranging only from 0.26 to 0.46 g cm^{-3} (Figure S1a,b; Table S2). LMA was not related to the variation in T_{leaf} (Figure S1b), cell wall thickness (T_{cw}; Figure S1c) nor chloroplast surface area exposed to intercellular air space per leaf area (S_c/S), neither considering species from this study only, nor considering also the species from Veromann-Jürgenson *et al.* (2017) (Figure S1d).

In contrast to LMA, significant correlations were found between g_{m_FLU} and the anatomical traits S_c/S and T_{cw} (Figure 2). A significant positive logarithmic correlation ($r^2 = 0.31$, $P < 0.05$) was found between g_{m_FLU} and S_c/S only when considering both species from this study and species measured in Veromann-Jürgenson *et al.* (2017) (Figure 2a), as S_c/S were the average values from this study and generally higher than those of Veromann-

Table 1 Photosynthetic characteristics for the gymnosperm species

Species	A_N (μmol m^{-2} sec^{-1})	g_s (mol CO_2 m^{-2} sec^{-1})	g_{m_FLU} (mol CO_2 m^{-2} sec^{-1})	C_i (μmol CO_2 mol^{-1} air)	C_c (μmol CO_2 mol^{-1} air)	R_d (μmol CO_2 m^{-2} sec^{-1})
Chamaecyparis obtusa	4.3 ± 0.3	0.033 ± 0.004	0.065 ± 0.017	211 ± 27	115 ± 12	0.8 ± 0.1
Juniperus oxycedrus	6.3 ± 1.1	0.059 ± 0.013	0.047 ± 0.015	272 ± 16	111 ± 19	1.3 ± 0.3
Picea glauca	7.6 ± 0.5	0.056 ± 0.006	0.049 ± 0.006	245 ± 13	86 ± 3	1.6 ± 0.3
Sequoiadendron giganteum	8.7 ± 1.3	0.095 ± 0.013	0.076 ± 0.012	292 ± 6	169 ± 27	1.6 ± 0.3
Taxus baccata	9.2 ± 0.4	0.062 ± 0.007	0.104 ± 0.025	231 ± 20	125 ± 13	0.7 ± 0.1
Taxus cuspidata	8.0 ± 0.6	0.056 ± 0.006	0.086 ± 0.011	236 ± 9	137 ± 9	0.9 ± 0.0
Thuja plicata	7.4 ± 0.7	0.055 ± 0.005	0.062 ± 0.011	247 ± 8	110 ± 7	1.8 ± 0.2

Average values ± SE (n = 3–7) are shown for net assimilation (A_N), stomatal conductance to CO_2 (g_s), mesophyll conductance calculated with the variable J method (g_{m_FLU}), substomatal CO_2 concentration (C_i), chloroplastic CO_2 concentration (C_c) and dark respiration rate (R_d).

Jürgenson *et al*. (2017) species. Regarding the relationship between g_{m_FLU} and T_{cw} (Figure 2b), no correlation was found when considering all gymnosperm species, which were located in the asymptote region of the significant exponential decay regression obtained when considering data from all spermatophyte species compiled by Onoda *et al*. (2017) (Figure 2b inset). Instead, mainly because of the narrow range of g_m values in gymnosperms (plus scattering due to the inherent uncertainties of the method used for its estimation, see Pons *et al*., 2009), two inverse linear regressions with no likely biological meaning were reported by considering the species from the current study (r^2 = 0.59, P < 0.05) and the species studied in Veromann-Jürgenson *et al*. (2017) (r^2 = 0.38, P < 0.05). Moreover, the positive correlation found here is largely dependent on the position of the two *Taxus* species in the relationship. Based on the structural limitation analysis of g_m performed after the estimation of the gas- and liquid-phase conductances following Tosens *et al*. (2016), the estimated gas-phase limitation in the mesophyll was between 8.0% and 20.5%, as the g_m of gymnosperm was mainly limited by liquid-phase components (Figure 3a). Among the different liquid-phase limitations, cell wall limitation (l_{cw}) was the predominant g_m constraint for all species (ranging from 65.9% to 80.9%) except for *T. baccata*, whose l_{cw} was of 31.9 ± 6.9%. Chloroplast stroma limitation (l_{st}) was the second limitation in importance (except in *T. baccata*, which was 47.1 ± 4.6%), whereas plasma membrane, cytoplasm and chloroplast envelope played only a minor role (Figure 3b). In this study, g_m modelled from anatomical characteristics (g_{m_ANAT}) using a common cell wall effective diffusivity (p_{cw}) of 0.028 m^3 m^{-3} (Tomás *et al*., 2013) did not correlate with g_{m_FLU} (Figure S2).

Cell wall composition in relation to leaf morphoanatomy and physiology

Cell wall extractions, considered as alcohol insoluble residues (AIR), per total leaf dry weight as well as the AIR's weight fraction of hemicelluloses, celluloses and pectins were determined for the seven gymnosperm species (Table 2). AIR ranged from 0.425 ± 0.026 g g^{-1} in *T. baccata* to 0.870 ± 0.042 g g^{-1} in *J. oxycedrus*. Their hemicelluloses content ranged from 180 ± 7 μg glucose mg^{-1} AIR in *T. cuspidata* to 357 ± 35 μg glucose mg^{-1} AIR in *P. glauca*; cellulose content ranged from 98 ± 9 μg glucose mg^{-1} AIR in *T. baccata* to 341 ± 9 μg glucose mg^{-1} AIR in *J. oxycedrus*, and the content of pectins ranged only from 48 ± 3 μg galacturonic acid mg^{-1} AIR in *T. cuspidata* to 65 ± 5 μg galacturonic acid mg^{-1} AIR in *S. giganteum*. Area-based cell wall components were calculated as X_{area} = X_{mass}/LMA to relate them to area-based A_N and g_m properly. Neither AIR nor the main area-based cell wall components (considering them separately, the sum of the 3, or the ratio pectins/(cellulose + hemicellulose)) were correlated with LMA (P > 0.1), probably associated with the interspecific leaf-shape variability. Instead, significant negative linear correlations between hemicelluloses and pectins and T_{cw} were found (r^2 = 0.69, P < 0.05 and r^2 = 0.65, P < 0.05, respectively) although not with celluloses (Figure 4). Neither AIR content nor main cell wall component concentrations correlated with net photosynthesis (Figure 5a,b). Conversely, g_{m_FLU} was negatively correlated with AIR (r^2 = 0.76, P < 0.01; Figure 5c), as well as hemicellulose (r^2 = 0.90, P < 0.005) and cellulose concentrations (r^2 = 0.68, P < 0.05; Figure 5d). Although absolute pectin concentration did not significantly correlate with g_m (r^2 = 0.55, P < 0.1; Figure 5d), pectin relative concentration expressed as the area-based pectins/(cellulose + hemicellulose) ratio was tightly correlated with g_m (r^2 = 0.94, P < 0.005; Figure 6).

DISCUSSION

Here we demonstrate that interspecific variations in mesophyll conductance to CO_2 (g_m) may be strongly influenced by differences in cell wall composition. In addition, we provide insight into the relationship between mesophyll cell

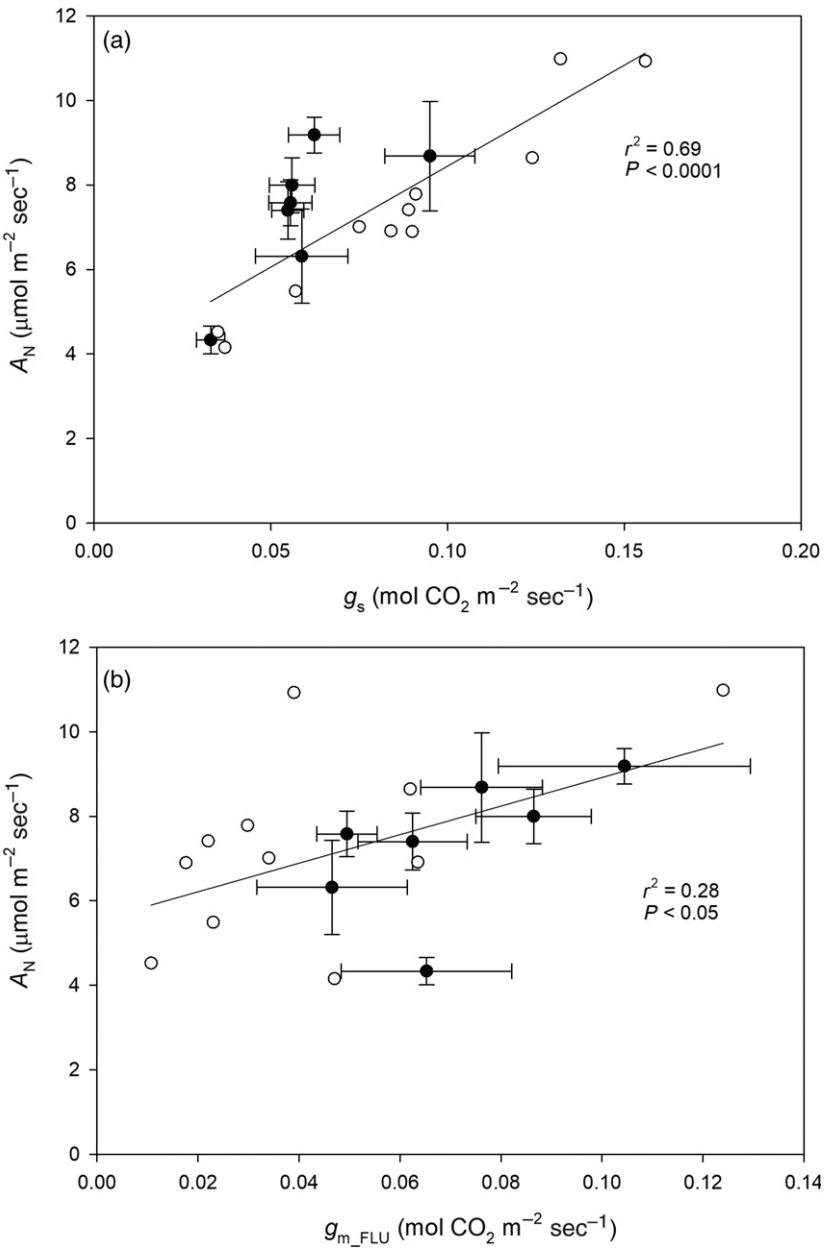

Figure 1. Photosynthesis relationship with stomatal and mesophyll conductance to CO_2.
Net photosynthesis (A_N) in relation to (a) stomatal conductance to CO_2 (g_s) and (b) mesophyll conductance to CO_2 estimated by chlorophyll fluorescence (g_{m_FLU}). Each point corresponds to one species (n = 3–7). Species from this study are marked as filled circles, while gymnosperm species from Veromann-Jürgenson *et al.* (2017) are marked as open circles. Filled circles with error bars display average ± SE values for the seven species considered in the present study. Linear regressions were fitted to the data.

wall thickness (T_{cw}) and composition. Our results show that higher relative but not absolute pectin concentration may have a major role in determining the maximum g_m in species with thick cell walls as gymnosperms. Such a role is independent to T_{cw}, and probably related to setting the effective CO_2 diffusivity of the cell wall. Finally, we discuss the potential mechanical link that would explain the observed relationships between cell wall composition and CO_2 diffusion resistance.

We performed a comprehensive analysis in seven gymnosperms covering the 60% of the T_{cw} variation range reported for spermatophytes (from 0.372 to 1.033 μm; Table S3, Figure 2b). Our aim was to explore the g_m regulation within the upper range of T_{cw} interspecific variation, within which increases in thickness seem to have a comparatively minor effect on g_m (Figure 3b inset). As the gas-phase limitation of g_m was generally low in the studied species (Figure 3a), and the species with the largest T_{cw} did not show larger S_c/S (Figure 2; Tables S2 and S3), the relatively low impact on g_m of thicker cell walls over about 0.4 μm T_{cw} is probably not fully compensated by other mesophyll anatomical traits, but should be at least partially compensated by variable cell wall effective diffusivity. The observed lack of a tight agreement between g_m estimated from chlorophyll fluorescence (g_{m_FLU}) and g_m modelled from anatomical characteristics (g_{m_ANAT}) when

Table 2 Dry leaf mass per unit projected area (LMA), fresh- and dry mass-based leaf cell wall fraction considered as alcohol insoluble residues (AIR), and dry mass-based hemicellulose, cellulose and pectin fractions of AIR. Average value ± SE (n = 4) are shown for AIR and for each cell wall component

Species	LMA (g m^{-2})	AIR (g g^{-1} fresh weight)	AIR (g g^{-1} dry weight)	Hemicelluloses (μg glc mg^{-1} AIR)	Cellulose (μg glc mg^{-1} AIR)	Pectins (μg gal ac mg^{-1} AIR)
Chamaecyparis obtusa	228 ± 11	0.261 ± 0.013	0.606 ± 0.031	272 ± 4	154 ± 9	58 ± 3
Juniperus oxycedrus	197 ± 5	0.427 ± 0.023	0.870 ± 0.042	278 ± 11	341 ± 9	63 ± 2
Picea glauca	184 ± 6	0.256 ± 0.010	0.635 ± 0.024	357 ± 35	244 ± 11	55 ± 6
Sequoiadendron giganteum	245 ± 28	0.217 ± 0.037	0.585 ± 0.051	234 ± 4	159 ± 4	65 ± 5
Taxus baccata	148 ± 9	0.165 ± 0.010	0.425 ± 0.026	204 ± 16	98 ± 9	53 ± 5
Taxus cuspidata	207 ± 3	0.178 ± 0.016	0.436 ± 0.040	180 ± 7	103 ± 5	48 ± 3
Thuja plicata	201 ± 4	0.277 ± 0.026	0.713 ± 0.068	230 ± 9	177 ± 7	58 ± 1

glc, glucose; gal ac, galacturonic acid.

considering constant cell wall effective diffusivity (p_{cw}) also suggests the existence of a variable effective diffusivity (Figure S2).

Cell wall properties affecting CO_2 diffusion are determined by the cell wall composition and content, and the assembly, orientation and cross-linkage between components. Although leaf cell wall composition can be a suitable proxy to cell wall CO_2 diffusive properties thanks to the ease with which it can be determined in comparison with T_{cw} and p_{cw}, its relationships with both cell wall CO_2 diffusion resistance properties remain mostly unexplored. Recently, Ellsworth *et al*. (2018) using mutants, and Clemente-Moreno *et al*. (2019) and Roig-Oliver *et al*. (2020) inducing abiotic stresses in tobacco and grapevine, respectively, provided first insight in the intraspecific relationships between the dynamic regulation of cell wall composition and g_m in response to abiotic stresses. However, the relationships at the interspecific level between cell wall composition and g_m are still unknown. To this end, we analysed the total leaf cell wall content extracted, assumed as the AIR and the relative proportion of the three major constituents of the plant's primary cell wall: cellulose, hemicelluloses and pectins. Each of these components generally constitutes about 20%–40% of the wall weight in angiosperms, although this can vary significantly among species (Cosgrove, 2005; Caffall and Mohnen, 2009; Ochoa-Villareal *et al*., 2012; Tenhaken, 2014). For instance, while pectin is the single largest constituent of the cell wall in Arabidopsis (Zablackis *et al*., 1995), it is only about 2%–10% in grasses (Ochoa-Villareal *et al*., 2012). Lignins are the major cell wall component missing from the present analysis. However, they are mostly present in secondary walls of structural tissue (Poorter *et al*., 2009; Zhong *et al*., 2019), which are not directly involved in photosynthesis (Kuusk *et al*., 2018), and where they can account for 30%–40% of AIR in gymnosperms (Renault and Zwiazek, 1997; Mediavilla *et al*., 2008). Apart from lignins, other cell wall components such as proteins, phenolic residues that solubilize and starch may account for the percentage of AIR not related to cellulose, hemicellulose and pectins, which may be also influenced by a differential in the water content of the primary and secondary walls (see Pettolino *et al*., 2012; Petit *et al*., 2019).

In the present interspecific comparison of conifer species, we found that g_m was negatively correlated with the concentration of both cellulose and hemicellulose in cell walls, and unrelated with the concentration of pectins (Figure 5c,d). Besides this, the strongest correlation was found between the ratio pectins/(cellulose + hemicellulose) and g_m (Figure 6), suggesting that it is the proportion among these components rather than their absolute concentrations that regulates CO_2 diffusion through cell walls. It is perhaps surprising that the positive effect of pectins on g_m provided that pectins are the minority cell wall compound of the three analysed in these species, ranging from 8% of the total cellulose + hemicellulose + pectins in *Picea glauca* to 15% in *T. baccata* (Table 2). Pectins have been described as the embedding matrix components of cell walls. Several studies described that pectins decrease the sieve size and increase the complexity of the wall (Leucci *et al*., 2008, Houston *et al*., 2016). However, while this negatively affects the diffusion of macromolecules, it might not affect CO_2 diffusion, as the pore size of the cell walls is approximately an order of magnitude larger than the CO_2 molecules (Evans *et al*., 2009). Instead, pectins had been shown to exhibit hydrocolloid properties and to bind several times their own volume of water, competing with one another for available water-forming aqueous phases of their own, which results in phase separation processes (Schiraldi *et al*., 2012). Pectins have also been shown to reduce the bulk modulus of elasticity in grapevines (i.e. to increase the elasticity of cell walls in response to water pressures, Roig-

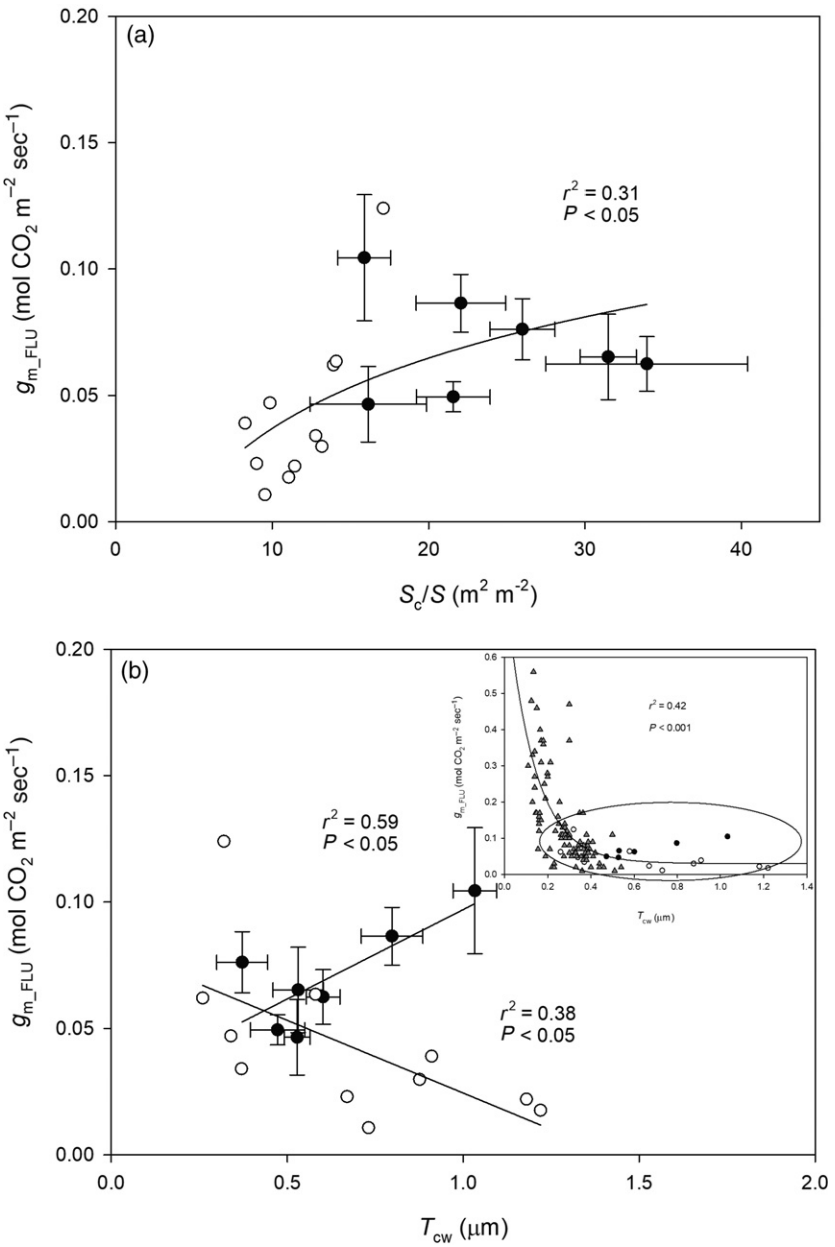

Figure 2. Mesophyll conductance to CO_2 relationship with key anatomical traits.
Mesophyll conductance to CO_2 estimated by chlorophyll fluorescence (g_{m_FLU}) in relation to (a) chloroplast surface area exposed to intercellular airspaces per projected leaf area (S_c/S), and (b) cell wall thickness (T_{cw}). Inset in (b) shows the general relationship observed between g_{m_FLU} and T_{cw} for vascular plants, with the relative position of gymnosperm species highlighted with an ellipse. Species from this study are marked as filled circles, gymnosperm species from Veromann-Jürgenson *et al.* (2017) are marked as open circles and data from spermatophytes species compiled by Onoda *et al.* (2017) are marked as orange triangles. Filled circles with error bars display average ± SE values (n = 3–7) for the seven species considered in the present study. Data were fitted in (a) by a logarithmic regression in considering all species, while data from each study were separately fitted by linear regression in (b).

Oliver *et al.*, 2020) and wall elasticity has been shown to be related to cell wall porosity in epidermal cells of Arabidopsis (Liu *et al.*, 2019). Therefore, we speculate that an increased fraction of pectins results in increased cell wall hydrophilicity and elasticity, thus increasing g_m because CO_2 molecules cross the wall dissolved in water. Alternatively, direct chemical interactions between cell wall components and CO_2 cannot be ruled out and specific studies are required to address this possibility. In either case, the effect of the pectins/(cellulose + hemicellulose) ratio on g_m might reflect an effect of cell wall composition in the effective diffusivity of cell walls.

Conclusions

The present study shows evidence for a correlation of the effect of cell wall composition on mesophyll CO_2 diffusion resistance in an interspecific comparison. Owing to their thick cell walls, gymnosperms are at the low end of the mesophyll conductance range reported for spermatophytes, but differences in cell wall composition correlated with differences in g_m within this range, probably reflecting an effect of composition on the effective diffusivity of the cell wall. The ratio of pectins to hemicelluloses and cellulose was tightly correlated with g_m, suggesting an active

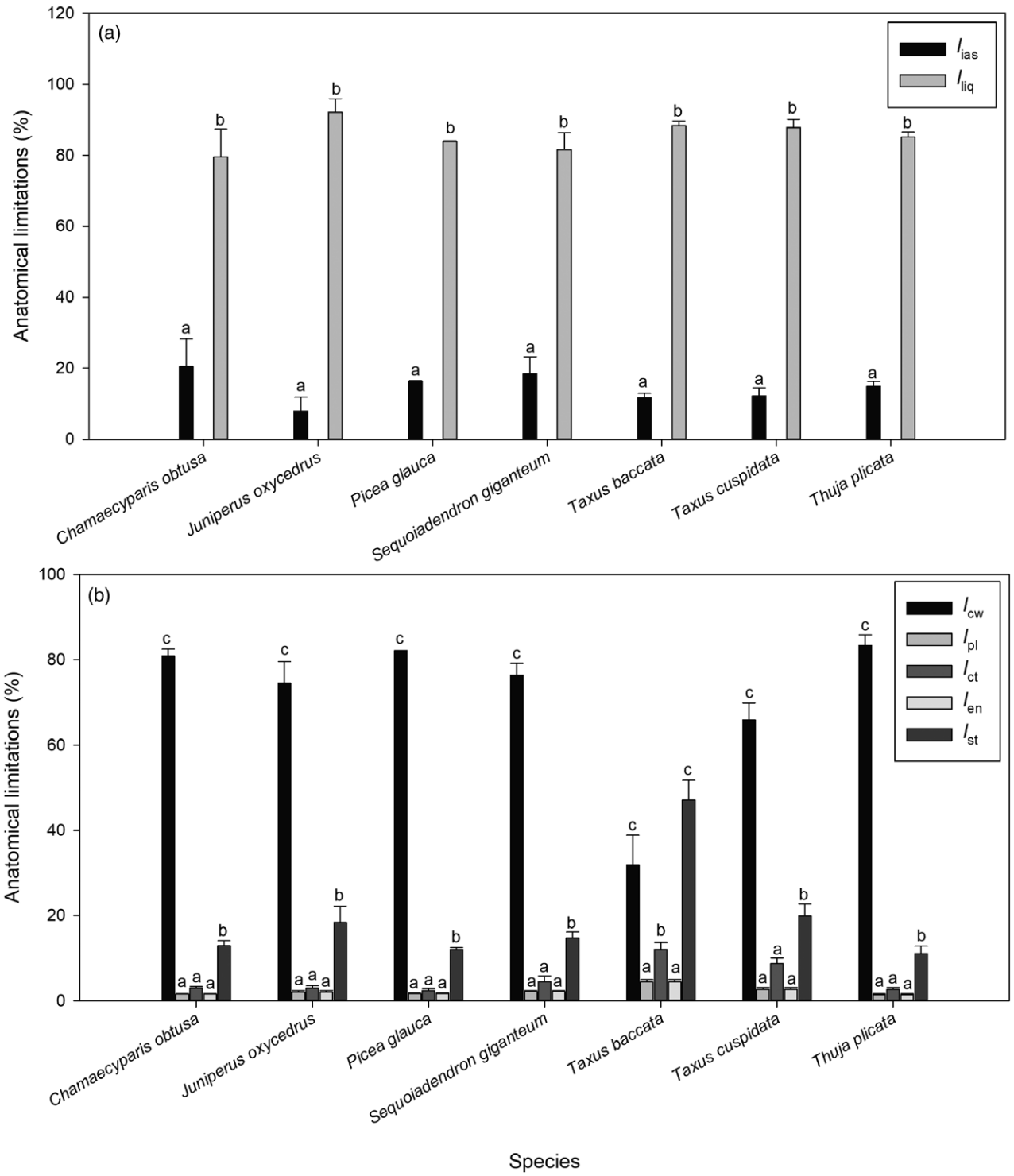

Figure 3. Anatomical limitations of mesophyll conductance to CO_2.
(a) Relative gas- and liquid-phase mesophyll conductance limitations (l_{ias} and l_{liq}, respectively) per species. (b) Relative limitation of liquid-phase components: cell wall (l_{cw}), plasma membrane (l_{pl}), cytoplasm (l_{ct}), chloroplast envelope (l_{en}) and stroma (l_{st}) on mesophyll conductance in each species. Error bars represent standard errors (n = 3–7). Different letters indicate significant differences between l_s, l_m and l_b at the 0.05 probability level based on Tukey's multiple comparison test.

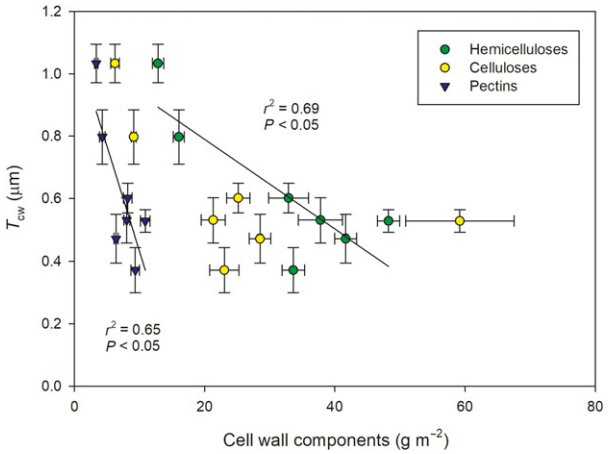

Figure 4. Relationship between cell wall thickness (T_{cw}) and cell wall components mass per leaf area. Data are means ± SE (n = 4) for each species. Cellulose and hemicellulose are expressed as grams of glucose equivalents per m^2, while pectins are expressed as grams of galacturonic acid equivalents per m^2. Linear regressions were fitted to the data.

but complex role of pectin relative content on the regulation of effective CO_2 diffusivity in the cell wall. The fact that pectins increase the hydrophilicity and hydraulic elasticity of cell walls, and that CO_2 molecules cross the cell wall dissolved in water, suggests that an increasing proportion of pectins to hemicelluloses and cellulose may increase the effective CO_2 diffusivity in cell walls to compensate the negative impact of thickened walls.

While these results represent an advance in our mechanistic understanding of g_m, more studies are needed on the relationship between cell wall composition and high plants to (i) improve the methodological protocol to determine the cell wall composition on mesophyll tissue only, to avoid the interference of cuticle, epidermal and vascular leaf tissue, and (ii) perform the analysis on different plant groups to confirm the existence of a general role of pectin proportion in setting effective CO_2 diffusivity in mesophyll cell walls. Moreover, similar studies in groups other than gymnosperms are needed to confirm this hypothesis, as there are important differences in the main cell wall components between land plant groups (Sarkar *et al.*, 2009; Popper *et al.*, 2011).

EXPERIMENTAL PROCEDURES

Plant material

Seven 40–70-cm tall plants of seven gymnosperm species were bought from a nursery. Plants were transplanted into pots (15 L, 30 cm pot diameter) containing 75:25 mixture of horticultural substrate (peat) and pearlite (granulometry A13) and fertilized with 5 g L^{-1} of slow release fertilizer (Multigreen; Haifa Chemicals, Madrid, Spain). Plants were grown outdoors fully exposed to direct sunlight at the University of the Balearic Islands (Mallorca, Spain) and watered by automatic drip every 3 days to maintain optimum water status and vigour. Measurements were performed in April 2016 with environmental conditions of 9.0–20.4°C mean min/max temperatures and 67.6% mean relative humidity. All measurements were performed on young fully expanded leaves to ensure mature leaf anatomy and to minimize variation between replicates.

Gas exchange and chlorophyll fluorescence measurement

Leaf gas exchange parameters were measured using a portable photosynthesis system (LI-6400; LI-COR, Inc., Nebraska, USA) with an infrared gas analyser coupled with a 2 cm^2 leaf fluorescence chamber (LI-6400-40 leaf chamber fluorometer; LI-COR, Inc.). Owing to the morphology and thickness of some species, the leaf chamber was sealed with a non-invasive putty-like adhesive (Blu Tack, Bostik) to avoid any major air leakage. All measurements were carried out between 10:00 and 17:00 h (central European summer time). The block temperature was fixed at 25°C, with air flow rate between 150 and 200 µmol min^{-1} to ensure the reliability of the measurements and VPD kept between 1.5 and 2.0 kPa for all measurements.

Leaves from randomly selected plants were fully characterized. Leaf steady-state conditions were induced at 400 µmol CO_2 mol^{-1} air and saturating photosynthetic photon flux density (PPFD 1500 µmol m^{-2} sec^{-1}, 90:10 red/blue light). Once steady-state conditions were achieved, typically after 30–40 min, complete light and CO_2 response curves at 21% O_2 and CO_2 response curves at 2% O_2 were performed in random order. Light response curves were measured at 400 µmol CO_2 mol^{-1} air at PPFD of 2000, 1500, 1000, 800, 600, 400, 200, 150, 100, 50 and 0 µmol m^{-2} sec^{-1}. CO_2 response curves were measured at PPFD 1500 µmol m^{-2} sec^{-1} at cuvette CO_2 concentration (C_a) of 400, 50, 100, 200, 300, 400, 600, 800, 1000, 1200, 1500, 2000 and 400 µmol mol^{-1}. Six to seven curves were performed per response curve type and per species on different individuals. The order in which curves were performed did not affect the responses. Values of A and steady-state fluorescence (F_s) were registered immediately after the steady-state conditions for gas exchange were achieved and then a saturating white light flash approximately 8000 µmol m^{-2} sec^{-1} was applied to determine the maximum fluorescence (F_m'). Multiphase flash methodology for chlorophyll fluorescence measurements was followed, as suggested by Loriaux *et al.* (2013), to avoid potential maximum yield underestimation error. The electron transport rate (ETR) was estimated from Genty *et al.* (1989) as ETR = PPFD × ΦPSII × α × β, where ΦPSII is the efficiency of photosystem II, α the leaf absorbance and β the electrons partitioning between photosystems I and II. ΦPSII was estimated as $\Phi PSII = (F_m' - F_s)/F_m'$ (Genty *et al.*, 1989). The α × β parameter was estimated following Valentini *et al.* (1995). Light response curves under non-photorespiratory conditions in a low O_2 atmosphere (<2%) were used to establish the relationship between ΦPSII and ΦCO_2 under non-photorespiratory conditions (with $\Phi CO_2 = (A + R_d)/PPFD$), then considering α × β = 4/b where b is the slope of the ΦPSII ~ ΦCO_2 relationship. Non-photorespiratory respiration during the day (R_d) was estimated as half the respiration rate measured after 2 h of darkness (Niinemets *et al.*, 2005; Martins *et al.*, 2013; Veromann-Jürgenson *et al.*, 2017). As gymnosperm leaves did not fully cover the 2 cm^2 cuvette, an image of the leaf fraction placed in the chamber was taken, and the actual area was calculated using ImageJ software (Wayne Rasband/NIH, Bethesda, MD, USA). The corrected areas were used to recalculate gas-exchange data. Moreover, any measurement performed at a non-ambient [CO_2] was corrected for leaks following Flexas *et al.* (2007). Then, g_m was estimated following Harley *et al.* (1992) as:

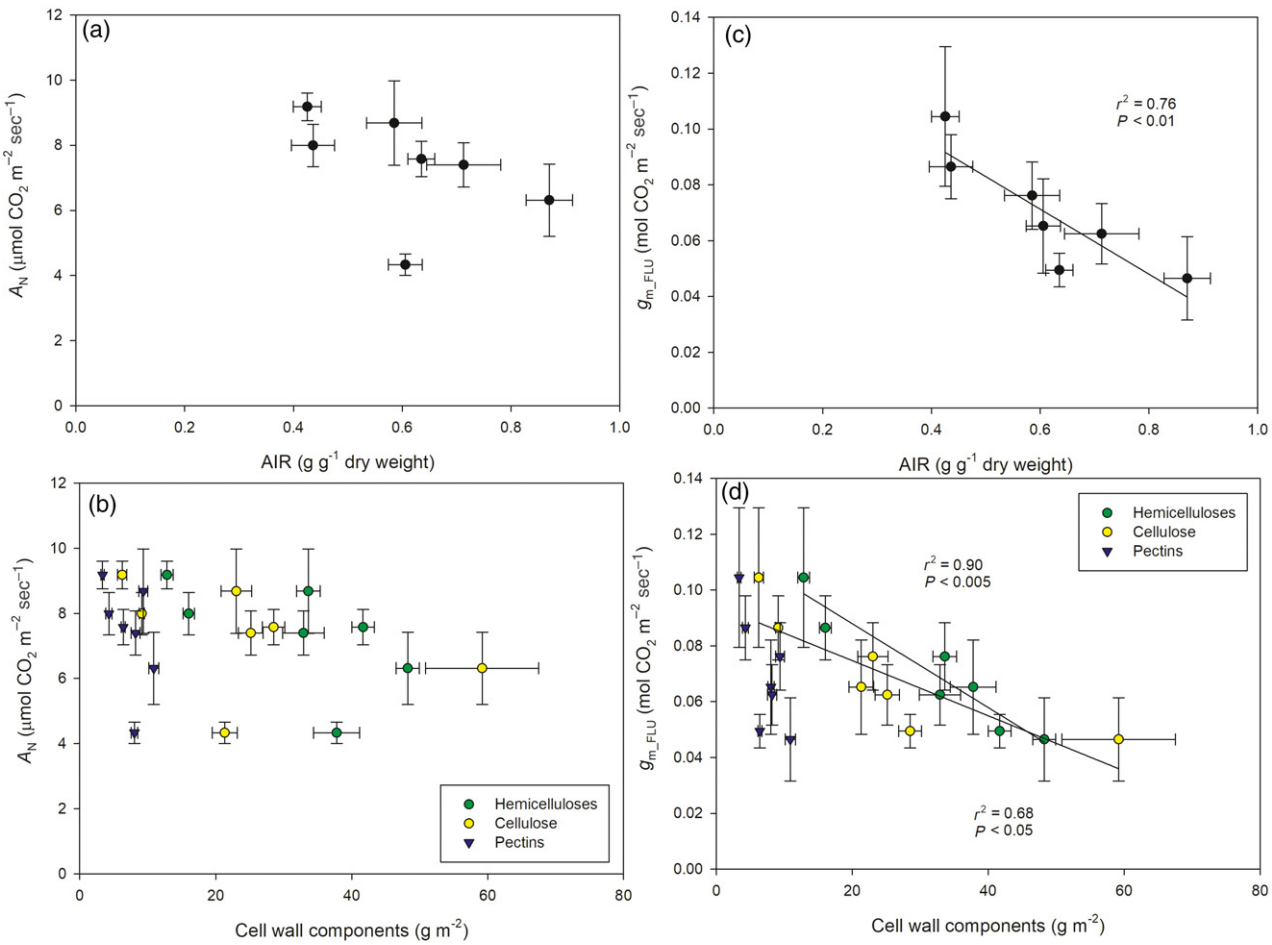

Figure 5. Photosynthesis and mesophyll conductance to CO_2 relationships between cell wall content and components. Relationship between net photosynthesis (A_N) and (a) the mass of cell walls prepared as alcohol insoluble residues per leaf dry weight (AIR) and (b) cell wall components mass per leaf area. Relationship between mesophyll conductance estimated by (c) chlorophyll fluorescence (g_{m_FLU}) and (d) AIR, and (e) cell wall components mass per leaf area. Cellulose and hemicellulose are expressed as grams of glucose equivalents per m^2, while pectins are expressed as grams of galacturonic acid equivalents per m^2. Data are means ± SE of four replicate measurements for each species. Linear regressions were fitted to the data.

$$g_{m\_FLU} = \frac{A_N}{C_i - \frac{\Gamma^*(ETR + p_2(A_N + R_d))}{(ETR - p_1(A_N + R_d))}} \quad (1)$$

where A is the net assimilation rate, Γ^* is CO_2 compensation point in absence of R_d, and C_i the CO_2 concentration in intercellular airspaces. Γ^* was assumed to be 42.5 µmol mol^{-1} as in Bernacchi *et al.* (2001) due to the absence of Γ^* values for gymnosperm species. Values of p_1 and p_2, which depend on the limited steps of ribulose bisphosphate regeneration, where assumed to be 4 and 8, respectively.

Anatomical measurements

Immediately after gas-exchange measurements, small leaf pieces (3 × 2 mm) of the area enclosed in the leaf chamber were cut off, immersed and fixed under vacuum pressure with a glutaraldehyde 4% and paraformaldehyde 2% in a 0.1 M phosphate buffer (pH 7.4) fixing solution. Five plants per species were sampled. Afterwards, samples were post-fixed in 2% buffered osmium tetroxide for 2 h and dehydrated in a graded series of ethanol. Dehydrated samples were embedded in resin (LR-White; London Resin Company, London, UK) and solidified in an oven at 60°C for at least 48 h.

Semi-thin cross-sections of 0.8 µm and ultrathin cross-sections of 90 nm for TEM were cut with an ultramicrotome (Leica UC6, Vienna, Austria). Semi-thin sections were dyed with 1% toluidine blue and observed at 200× magnifications under Olympus BX60 light microscopy (Olympus, Tokyo, Japan) and photographed with a Moticam 3 (Motic Electric Group Co., Xiamen, China). The ultrathin sections were contrasted with uranyl acetate and lead citrate and viewed at 1200× and 30 000× magnifications with TEM (TEM H600; Hitachi, Tokyo, Japan). All images were analysed using IMAGEJ software (Schneider *et al.*, 2012). From light microscopy images leaf thickness (T_{leaf}), mesophyll thickness (T_{mes}), number of palisade layers, fraction of the mesophyll occupied by intercellular airspaces (f_{ias}) and mesophyll surface area exposed to intercellular airspace (S_m/S) were measured. From TEM images, the cell wall thickness (T_{cw}), cytoplasm thickness (T_{cyt}), chloroplast length (L_{chl}), chloroplast thickness (T_{chl}) and chloroplast surface area exposed to intercellular airspace (S_c/S) were measured and calculated following Tomás *et al.* (2013). The cell curvature correction factor was

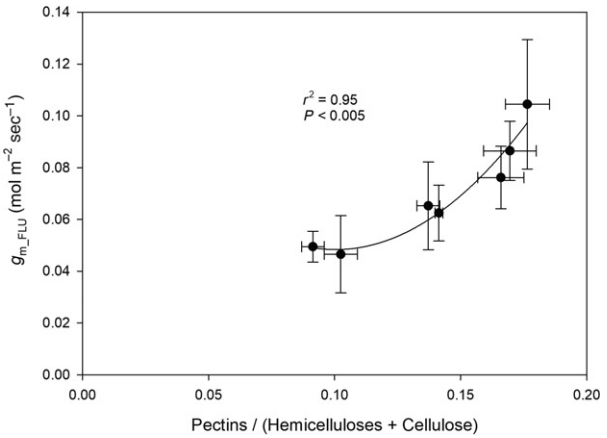

Figure 6. Relationship between mesophyll conductance estimated by chlorophyll fluorescence (g_{m_FLU}) and the ratio of pectins to hemicelluloses and celluloses. Polynomial regression was fitted to the data.

calculated according to Thain (1983). Factors between 1.18 and 1.26 and between 1.37 and 1.48 were applied to cell surface area estimates for mesophyll spongy (oblate spheroids) and palisade cells (prolate spheroids), respectively. Four to six randomly selected different fields of view were considered per plant replicate to measure each anatomical characteristic. For each type of mesophyll tissue (spongy and palisade), 10 measurements were made for T_{leaf}, T_{mes}, f_{ias}, T_{cw}, S_m/S and S_c/S, and 15 measurements per mesophyll type were made for L_{chl} and T_{chl}. Then, weighted averages based on tissue volume fractions were calculated.

Estimation of mesophyll conductance modelled from anatomical characteristics

The one-dimensional within-leaf gas diffusion model of Niinemets and Reichstein (2003) modified by Tomás *et al.* (2013) was applied. Mesophyll diffusion conductance as a composite conductance for within-leaf gas, liquid and lipid components is given as:

$$g_{m\_ANAT} = \frac{1}{\frac{1}{g_{ias}} + \frac{RT_k}{H \cdot g_{liq}}} \quad (2)$$

where H is the Henry's law constant (m^3 mol^{-1} K^{-1}), R is the gas constant (Pa m^3 K^{-1} mol^{-1}) and T_k is the absolute temperature (K). $H/(RT_k)$ is the dimensionless form of Henry's law constant needed to convert a liquid- and lipid-phase conductance (g_{liq} and g_{lip}) into a gas-phase equivalent conductance (Niinemets and Reichstein, 2003). Gas-phase diffusion depends on the fraction of mesophyll volume occupied by intercellular air spaces (f_{ias}, m^3 m^{-3}), and the effective diffusion path length in the gas phase (ΔL_{ias}) (Syvertsen *et al.*, 1995; Terashima *et al.*, 2011):

$$g_{ias} = \frac{D_a \cdot f_{ias}}{\Delta L_{ias} \cdot \varsigma} \quad (3)$$

where ς is the diffusion path tortuosity (m m^{-1}) and D_a (m^2 sec^{-1}) is the diffusion coefficient for CO_2 in the gas phase (1.51·10^{-5} m^2 sec^{-1} at 22°C). ΔL_{ias} was approximated by mesophyll thickness divided by two (Niinemets and Reichstein, 2003). An estimate of ς was used as a default value of 1.57 m m^{-1} (Niinemets and Reichstein, 2003; Syvertsen *et al.*, 1995). The total liquid-phase conductance is provided by the sum of the inverse of serial conductances:

$$\frac{1}{g_{liq}} = \left(\frac{1}{g_{cw}} + \frac{1}{g_{pl}} + \frac{1}{g_{ct}} + \frac{1}{g_{en}} + \frac{1}{g_{st}}\right) \cdot S_c/S \quad (4)$$

where partial conductances account for cell wall (g_{cw}), plasmalemma (g_{pl}), cytosol (g_{ct}), chloroplast envelope (g_{en}) and chloroplast stroma (g_{st}). The cell wall, cytosol and stromal conductances are given by a general equation:

$$g_i = \frac{r_{f,i} \cdot D_w \cdot p_i}{\Delta L_i} \quad (5)$$

where g_i (m sec^{-1}) is either g_{cw}, g_{ct} or g_{st}, ΔL_i (m) is the diffusion path length and p_i (m^3 m^{-3}) is the effective diffusivity in the given part of the diffusion pathway, D_w is the aqueous-phase diffusion coefficient for CO_2 (1.79 10^{-9} m^2 sec^{-1} at 25°C) and the dimensionless factor $r_{f,i}$ accounts for the decrease of diffusion conductance compared to free diffusion in water (Weisiger, 1998). For cell walls where the aqueous-phase diffusion has been shown to approximate free water, $r_{f,i}$ = 1 (Rondeau-Mouro *et al.*, 2008). The value of r_f was set at 0.3 for g_{ct} and g_{st} to account for the reduction of diffusion conductance due to high concentrations of high molecular solutes and intracellular (cytoskeleton) and intraorganellar (thylakoids) heterogeneities (Niinemets and Reichstein, 2003). Effective diffusivity, p_i, was taken as 1 for g_{ct} and g_{st}. Cell wall porosity (p_{cw}) was taken as 0.028, as applied by Tomás *et al.* (2013) for species with species with T_{cw} > 0.4 μm. Conductance in units of m sec^{-1} can be converted into molar units considering that

$$g[\text{mol m}^{-2}\text{ sec}^{-1}] = g[\text{m sec}^{-1}]44.6[273.16/(273.16 + T_L)(P/101.325)],$$

where T_L is the leaf temperature (°C) and P (Pa) is the air pressure. Owing to the difficulty in measuring the thickness of the plasma membrane, the chloroplast envelope and the limited information about the permeability of the lipid-phase membranes, g_{pl} and g_{env} were assumed as constant values (0.0035 m sec^{-1}) as previously suggested in other studies (Evans *et al.*, 1994; Peguero-Pina *et al.*, 2012; Tosens *et al.*, 2012a,b; Tomás *et al.*, 2013).

Analysis of quantitative limitations of A_N and g_m

The *relative* limitations on A_N for gymnosperms were calculated following Grassi and Magnani (2005). This analysis quantifies the relative importance of stomatal, mesophyll conductance and biochemical limitations [the latter integrating both Rubisco and photochemistry/Calvin cycle, because photosynthesis operates at co-limitation between these two factors; see Gallé *et al.* (2009) and Varone *et al.* (2012) for further explanation]. *Relative* limitations, that is, those imposed by stomatal (l_s) or mesophyll conductance (l_{mc}), and biochemical capacity (l_b), were calculated as:

$$l_s = \frac{\frac{g_{tot}}{g_s} \cdot \frac{\delta A_N}{\delta C_c}}{g_{tot} + \frac{\delta A_N}{\delta C_c}} \quad (6)$$

$$l_m = \frac{\frac{g_{tot}}{g_m} \cdot \frac{\delta A_N}{\delta C_c}}{g_{tot} + \frac{\delta A_N}{\delta C_c}} \quad (7)$$

$$l_b = \frac{g_{tot}}{g_{tot} + \frac{\delta A_N}{\delta C_c}} \quad (8)$$

where g_s and g_{m_FLU} are the stomatal and mesophyll conductances to CO_2 and g_{tot} is the total conductance (the sum of inversed serial conductances g_{m_FLU} and g_s). $\delta A_N/\delta C_c$ is the slope of A_N/C_c response curves – estimated from 21% O_2 A/C_i curves

following Harley *et al.* (1992) – over a C_c range of 75–150 μmol mol^{-1}. These three values sum 100% and characterize the extent to which any of the three limitations curbs photosynthesis at the given values of the other two. The contribution of the gas-phase and the liquid-phase resistances, and then only of the different components of cellular resistance, to mesophyll resistance to CO_2 diffusion was estimated from the anatomical model following Tosens *et al.* (2016). This share of limitation (l_i) by different liquid-phase components was calculated as:

$$l_i = \frac{g_{m\_ANAT}}{g_i \cdot S_c/S} \quad (9)$$

where l_i is the limitation by the cell wall, the plasmalemma, cytosol, chloroplast envelope and stroma, and g_i refers to the diffusion conductance of each corresponding diffusion pathway. The limitation of each cellular component was scaled up with S_c/S.

Leaf mass per unit projected area and leaf density

Leaf portions similar to the measured leaves were taken, weighed to determine the fresh weight and photographed to determine leaf area. Afterwards, leaf portions were placed in an oven at 60°C until constant dry weight was reached to calculate the fresh-to-dry weight ratio and dry leaf mass per unit leaf projected area (LMA). Leaf density (D_{leaf}) was calculated as the LMA per T_{leaf} average values (Niinemets, 1999).

Cell wall composition determination

Leaves of four plants per species were sampled (approximately 1 g) for cell wall analysis. To minimize the leaf starch content, sampling was performed early in the morning, immediately frozen in liquid nitrogen and then stored for further analysis. Later, samples were boiled in absolute ethanol until bleached. Afterwards, to eliminate any alcohol soluble compound, samples were cleaned in acetone shaking for 30 min twice, and then, samples were air-dried and homogenized by dry milling. The resulting AIR, which represents the cell wall crude material, was treated with α-amylase (Sigma; St. Louis, MO, USA) overnight to remove the starch retained in the sample. After that iodine/potassium iodide staining was performed to ensure the samples were starch free. Then, samples were used for the polysaccharide compounds analysis. For each sample, 3 mg of AIR were hydrolysed with 2 M trifluoroacetic acid (TFA) for 1 h a 121°C and then centrifuged at 13 000 ***g*** for 10 min. Supernatant (non-cellulosic cell wall components, mainly hemicellulose and pectins) was separated and kept at 4°C, while precipitated (cellulosic cell wall components) was cleaned once in distilled water, twice in acetone and then air-dried. The dry fraction was hydrolysed with 200 μl sulfuric acid (72%) for 1 h at room temperature, diluted with distilled water to 6 ml (0.5 M sulfuric acid) and heated to 121°C for 2 h to obtain the total sugar corresponding to the cellulose fraction. Total sugars from both AIR fractions (hemicelluloses and celluloses from the soluble and insoluble 2 M TFA fraction, respectively) were separately determined with the phenol sulfuric colorimetric method (Dubois *et al.*, 1956) by considering glucose equivalents as standard in a Varioskan Lux (Thermo Scientific). Uronic acids (pectins) were quantified from the soluble 2 M TFA fraction by colorimetry (Blumenkrantz and Asboe-Hansen, 1973) using 2-hydroxydiphenyl as reagent and galacturonic acid as standard in a Varioskan Lux. All parameters were recalculated to a dry-weight basis by using the fresh-to-dry weight ratio and then transformed to a projected area basis as $X_{area} = X_{mass}/LMA$.

Statistical analysis

Pearson correlation matrices were determined to reveal the relationships between traits. Significances were distinguished at the $P < 0.05$, $P < 0.01$ and $P < 0.0001$ levels. One-way ANOVA analysis was used to test the differences in measured traits between species. The differences between means were detected by Tukey's honest significant difference tests ($P < 0.05$). These analyses were performed with the software package SPSS 11.0 (SPSS, Chicago, IL, USA).

ACKNOWLEDGEMENTS

This work was supported by the project CTM2014-53902-C2-1-P from the Ministerio de Economía y Competitividad (MINECO, Spain) and the ERDF (FEDER). MC acknowledges the predoctoral fellowship FPI/1700/2014 by Conselleria d'Educació, Cultura i Universitats (Govern de les Illes Balears) and European Social Fund, and MN acknowledges predoctoral fellowship BES-2015-072578 by Ministerio de Economía y Competitividad (MINECO, Spain) and European Social Fund. The authors are grateful to Miquel Truyols (Camp experimental, UIB) for his support to our experiment, to Mª Teresa Mínguez, Universitat de València (Secció Microscòpia Electrònica, SCSIE), and to Dr Ferran Hierro, Universitat de les Illes Balears (Serveis Cientificotècnics), for technical support during microscopic analyses. We acknowledge Antonio Molina for his helpful and constructive suggestions on the manuscript.

AUTHOR CONTRIBUTIONS

MC, MN and JF contributed to the conception and design of the experiments, MC, MN, MJC-M and EM contributed to the acquisition of data, MC, MN, MJC-M, JG, EM and JF contributed to data analysis and interpretation, MC, MN and JF drafted the manuscript, and all authors critically revised and approved the final version of the manuscript for publication.

CONFLICT OF INTEREST

The authors declare no conflicts of interest.

DATA AVAILABILITY STATEMENT

All relevant data can be found within the manuscript and its supporting materials.

SUPPORTING INFORMATION

Additional Supporting Information may be found in the online version of this article.

Figure S1. LMA in relation to morphoanatomical traits.

Figure S2. Correlation between mesophyll conductance estimates.

Table S1. Relative photosynthesis limitations

Table S2. Morphological and anatomical structural traits.

Table S3. Ultrastructural anatomic traits.

REFERENCES

Baron-Epel, O., Gharyal, P.K. and Schindler, M. (1988) Pectins as mediators of wall porosity in soybean cells. *Planta*, **175**, 389–395.

Bellincampi, D., Cervone, F. and Lionetti, V. (2014) Plant cell wall dynamics and wall-related susceptibility in plant-pathogen interactions. *Front. Plant Sci.* **5**, 228.

Bernacchi, C.J., Singsaas, E.L., Pimentel, C., Portis, A.R. and Long, S.P. (2001) Improved temperature response functions for models of Rubisco-limited photosynthesis. *Plant Cell Environ.* **24**, 253–259.

Blumenkrantz, N. and Asboe-Hansen, G. (1973) New method for quantitative-determination of uronic acids. *Anal. Biochem.* **54**, 484–489.

Caffall, K.H. and Mohnen, D. (2009) The structure, function, and biosynthesis of plant cell wall pectic polysaccharides. *Carbohydr. Res.* **344**, 1879–1900.

Carpita, N., Sabularse, D., Montezinos, D. and Delmer, D.P. (1979) Determination of the pore size of cell walls of living plant cells. *Science*, **205**, 1144–1147.

Carriquí, M., Cabrera, H.M., Conesa, M.À. *et al.* (2015) Diffusional limitations explain the lower photosynthetic capacity of ferns as compared with angiosperms in a common garden study. *Plant Cell Environ.* **38**, 448–460.

Carriquí, M., Douthe, C., Molins, A. and Flexas, J. (2019a) Leaf anatomy does not explain apparent short-term responses of mesophyll conductance to light and CO_2 in tobacco. *Physiol. Plant.* **165**, 604–618.

Carriquí, M., Roig-Oliver, M., Brodribb, T.J. *et al.* (2019b) Anatomical constraints to nonstomatal diffusion conductance and photosynthesis in lycophytes and bryophytes. *New Phytol.* **222**, 1256–1270.

Clemente-Moreno, M.J., Gago, J., Diaz-Vivancos, P. *et al.* (2019) The apoplastic antioxidant system and altered cell wall dynamics influence mesophyll conductance and the rate of photosynthesis. *Plant J.* **99**, 1031–1046.

Cosgrove, D.J. (2005) Growth of the plant cell wall. *Nat. Rev. Mol. Cell Biol.* **6**, 850–861.

Cosgrove, D.J. (2016) Plant cell wall extensibility: connecting plant cell growth with cell wall structure, mechanics, and the action of wall-modifying enzymes. *J. Exp. Bot.* **67**, 463–476.

Cosgrove, D.J. and Jarvis, M.C. (2012) Comparative structure and biomechanics of plant primary and secondary cell walls. *Front. Plant Sci.* **3**, 204.

Cousins, A.B., Mullendore, D.L. and Sonawane, B.V. (2020) Recent developments in mesophyll conductance in C3, C4, and crassulacean acid metabolism plants. *Plant J.* **101**, 816–830.

Dubois, M., Gilles, K.A., Hamilton, J.K., Rebers, P.A. and Smith, F. (1956) Colorimetric method for determination of sugars and related substances. *Anal. Chem.* **28**, 350–356.

Ellsworth, P.V., Ellsworth, P.Z., Koteyeva, N.K. and Cousins, A.B. (2018) Cell wall properties in *Oryza sativa* influence mesophyll CO_2 conductance. *New Phytol.* **219**, 66–76.

Evans, J.R., Kaldenhoff, R., Genty, B. and Terashima, I. (2009) Resistances along the CO_2 diffusion pathway inside leaves. *J. Exp. Bot.* **60**, 2235–2248.

Evans, J.R., Voncaemmerer, S., Setchell, B.A. and Hudson, G.S. (1994) The relationship between CO_2 transfer conductance and leaf anatomy in transgenic tobacco with a reduced content of Rubisco. *Aust. J. Plant Physiol.* **21**, 475–495.

Fleischer, A., O'Neill, M.A., Ehwald, R. (1999) The pore size of non-graminaceous plant cell walls is rapidly decreased by borate ester cross-linking of the pectic polysaccharide rhamnogalacturonan II. *Plant Physiol.* **121**, 829–838.

Flexas, J., Barbour, M.M., Brendel, O. *et al.* (2012) Mesophyll diffusion conductance to CO_2: an unappreciated central player in photosynthesis. *Plant Sci.* **193**, 70–84.

Flexas, J., Cano, F.J., Carriquí, M. *et al.* (2018) CO2 Diffusion Inside Photosynthetic Organs. *The Leaf: A Platform for Performing Photosynthesis*. Cham: Springer.

Flexas, J. and Carriquí, M. (2020) Photosynthesis and photosynthetic efficiencies along the terrestrial plant's phylogeny: lessons for improving crop photosynthesis. *Plant J.* **101**, 964–978.

Flexas, J., Díaz-Espejo, A., Berry, J.A. *et al.* (2007) Analysis of leakage in IRGA's leaf chambers of open gas exchange systems: quantification and its effects in photosynthesis parameterization. *J. Exp. Bot.* **58**, 1533–1543.

Gago, J., Carriqui, M., Nadal, M. *et al.* (2019) Photosynthesis optimized across land plant phylogeny. *Trends Plant Sci.* **24**, 947–958.

Gago, J., Daloso Dde, M., Figueroa, C.M., Flexas, J., Fernie, A.R. and Nikoloski, Z. (2016) Relationships of leaf net photosynthesis, stomatal conductance, and mesophyll conductance to primary metabolism: a multispecies meta-analysis approach. *Plant Physiol.* **171**, 265–279.

Gago, J., Daloso, D.M., Carriqui, M., Nadal, M., Morales, M., Araújo, W.L., Nunes-Nesi, A. and Flexas, J. (2020) Mesophyll conductance: the leaf corridors for photosynthesis. *Biochem. Soc. Trans.* **48**, 429–439.

Gallé, A., Florez-Sarasa, I., Tomás, M. *et al.* (2009) The role of mesophyll conductance during water stress and recovery in tobacco (*Nicotiana sylvestris*): acclimation or limitation? *J. Exp. Bot.* **60**, 2379–2390.

Genty, B., Briantais, J.M. and Baker, N.R. (1989) The relationship between the quantum yield of photosynthetic electron-transport and quenching of chlorophyll fluorescence. *Biochim. Biophys. Acta*, **990**, 87–92.

Grassi, G. and Magnani, F. (2005) Stomatal, mesophyll conductance and biochemical limitations to photosynthesis as affected by drought and leaf ontogeny in ash and oak trees. *Plant Cell Environ.* **28**, 834–849.

Han, J., Lei, Z., Flexas, J. *et al.* (2018) Mesophyll conductance in cotton bracts: anatomically determined internal CO_2 diffusion constraints on photosynthesis. *J. Exp. Bot.* **69**, 5433–5443.

Harley, P.C., Loreto, F., Dimarco, G. and Sharkey, T.D. (1992) Theoretical considerations when estimating the mesophyll conductance to CO_2 flux by analysis of the response of photosynthesis to CO_2. *Plant Physiol.* **98**, 1429–1436.

Houston, K., Tucker, M.R., Chowdhury, J., Shirley, N. and Little, A. (2016) The plant cell wall: a complex and dynamic structure as revealed by the responses of genes under stress conditions. *Front. Plant Sci.* **7**, 984.

Kuusk, V., Niinemets, U. and Valladares, F. (2018) A major trade-off between structural and photosynthetic investments operative across plant and needle ages in three Mediterranean pines. *Tree Physiol.* **38**, 543–557.

Lawson, T. and Flexas, J. (2020) Fuelling life: recent advances in photosynthesis research. *Plant J.* **101**, 753–755.

Leucci, M.R., Lenucci, M.S., Piro, G. and Dalessandro, G. (2008) Water stress and cell wall polysaccharides in the apical root zone of wheat cultivars varying in drought tolerance. *J. Plant Physiol.* **165**, 1168–1180.

Liu, X., Li, J., Zhao, H. *et al.* (2019) Novel tool to quantify cell wall porosity relates wall structure to cell growth and drug uptake. *J. Cell Biol.* **218**, 1408–1421.

Loriaux, S.D., Avenson, T.J., Welles, J.M. *et al.* (2013) Closing in on maximum yield of chlorophyll fluorescence using a single multiphase flash of sub-saturating intensity. *Plant Cell Environ.* **36**, 1755–1770.

Maron, L. (2019) Rethinking our models of the plant cell wall. *Plant J.* **100**, 1099–1100.

Martins, S.C., Galmes, J., Molins, A. and Damatta, F.M. (2013) Improving the estimation of mesophyll conductance to CO_2: on the role of electron transport rate correction and respiration. *J. Exp. Bot.* **64**, 3285–3298.

Mccann, M.C., Wells, B. and Roberts, K. (1990) Direct visualization of cross-links in the primary plant-cell wall. *J. Cell Sci.* **96**, 323–334.

Mediavilla, S., Garcia-Ciudad, A., Garcia-Criado, B. and Escudero, A. (2008) Testing the correlations between leaf life span and leaf structural reinforcement in 13 species of European Mediterranean woody plants. *Funct. Ecol.* **22**, 787–793.

Miyazawa, S.I. and Terashima, I. (2001) Slow development of leaf photosynthesis in an evergreen broad-leaved tree, *Castanopsis sieboldii*: relationships between leaf anatomical characteristics and photosynthetic rate. *Plant Cell Environ.* **24**, 279–291.

Momayyezi, M. and Guy, R.D. (2017) Substantial role for carbonic anhydrase in latitudinal variation in mesophyll conductance of *Populus trichocarpa* Torr. & Gray. *Plant Cell Environ.* **40**, 138–149.

Momayyezi, M., Mckown, A.D., Bell, S.C.S. and Guy, R.D. (2020) Emerging roles for carbonic anhydrase in mesophyll conductance and photosynthesis. *Plant J.* **101**, 831–844.

Morales, L.V., Coopman, R.E., Rojas, R. *et al.* (2014) Acclimation of leaf cohorts expanded under light and water stresses: an adaptive mechanism of *Eucryphia cordifolia* to face changes in climatic conditions? *Tree Physiol.* **34**, 1305–1320.

Muir, C.D., Hangarter, R.P., Moyle, L.C. and Davis, P.A. (2014) Morphological and anatomical determinants of mesophyll conductance in wild relatives of tomato (*Solanum* sect. Lycopersicon, sect. Lycopersicoides; Solanaceae). *Plant Cell Environ.* **37**, 1415–1426.

Niinemets, U. (1999) Components of leaf dry mass per area - thickness and density - alter leaf photosynthetic capacity in reverse directions in woody plants. *New Phytol.* **144**, 35–47.

Niinemets, U., Cescatti, A., Rodeghiero, M. and Tosens, T. (2005) Leaf internal diffusion conductance limits photosynthesis more strongly in older leaves of Mediterranean evergreen broad-leaved species. *Plant Cell Environ.* **28**, 1552–1566.

Niinemets, U. and Reichstein, M. (2003) Controls on the emission of plant volatiles through stomata: differential sensitivity of emission rates to stomatal closure explained. *J. Geophys. Res.* **108**, 4208.

Nobel, P.S. (2004) *Physicochemical and Environmental Plant Physiology*. Burlington, MA: Elsevier Academic Press.

Ochoa-Villareal, M., Aispuro-Hernández, E., Vargas-Aispuro, I. and Martínez-Téllez, M.Á. (2012) Plant cell wall polymers: function, structure and biological activity of their derivatives. In *Polymerization* (Gomes, D.S., ed). InTech: Rijeka.

Onoda, Y., Wright, I.J., Evans, J.R. *et al.* (2017) Physiological and structural tradeoffs underlying the leaf economics spectrum. *New Phytol.* **214**, 1447–1463.

Peguero-Pina, J.J., Flexas, J., Galmes, J. *et al.* (2012) Leaf anatomical properties in relation to differences in mesophyll conductance to CO_2 and photosynthesis in two related Mediterranean *Abies* species. *Plant Cell Environ.* **35**, 2121–2129.

Peguero-Pina, J.J., Siso, S., Flexas, J. *et al.* (2017) Coordinated modifications in mesophyll conductance, photosynthetic potentials and leaf nitrogen contribute to explain the large variation in foliage net assimilation rates across *Quercus ilex* provenances. *Tree Physiol.* **37**, 1084–1094.

Petit, J., Gulisano, A., Dechesne, A. and Trindade, L.M. (2019) Phenotypic variation of cell wall composition and stem morphology in hemp (*Cannabis sativa* L.): optimization of methods. *Front. Plant Sci.* **10**, 959.

Pettolino, F.A., Walsh, C., Fincher, G.B. and Bacic, A. (2012) Determining the polysaccharide composition of plant cell walls. *Nat. Protoc.* **7**, 1590–1607.

Pons, T.L., Flexas, J., Von Caemmerer, S. *et al.* (2009) Estimating mesophyll conductance to CO_2: methodology, potential errors, and recommendations. *J. Exp. Bot.* **60**, 2217–2234.

Poorter, H., Niinemets, U., Poorter, L., Wright, I.J. and Villar, R. (2009) Causes and consequences of variation in leaf mass per area (LMA): a meta-analysis. *New Phytol.* **182**, 565–588.

Popper, Z.A., Michel, G., Herve, C. *et al.* (2011) Evolution and diversity of plant cell walls: from algae to flowering plants. *Annu. Rev. Plant Biol.* **62**, 567–590.

Read, S.M., and Bacic, A. (1996) Cell wall porosity and its determination. In *Plant cell wall analysis. Modern methods of plant analysis* (Linskens H.F., and Jackson J.F., eds). vol **17**. Berlin: Springer.

Ren, T., Weraduwage, S.M. and Sharkey, T.D. (2019) Prospects for enhancing leaf photosynthetic capacity by manipulating mesophyll cell morphology. *J. Exp. Bot.* **70**, 1153–1165.

Renault, H., Roussel, V., El Amrani, A. *et al.* (2010) The Arabidopsis pop2-1 mutant reveals the involvement of GABA transaminase in salt stress tolerance. *BMC Plant Biol.* **10**, 20.

Renault, S. and Zwiazek, J.J. (1997) Cell wall composition and elasticity of dormant and growing white spruce (*Picea glauca*) seedlings. *Physiol. Plant.* **101**, 323–327.

Roig-Oliver, M., Nadal, M., Clemente-Moreno, M.J., Bota, J. and Flexas, J. (2020) Cell wall components regulate photosynthesis and leaf water relations of Vitis vinifera cv. Grenache acclimated to contrasting environmental conditions. *J. Plant Physiol.* **244**, 153084.

Rondeau-Mouro, C., Defer, D., Leboeuf, E. and Lahaye, M. (2008) Assessment of cell wall porosity in *Arabidopsis thaliana* by NMR spectroscopy. *Int. J. Biol. Macromol.* **42**, 83–92.

Sarkar, P., Bosneaga, E. and Auer, M. (2009) Plant cell walls throughout evolution: towards a molecular understanding of their design principles. *J. Exp. Bot.* **60**, 3615–3635.

Schiraldi, A., Fessas, D. and Signorelli, M. (2012) Water activity in biological systems – a review. *Polish J. Food Nutr. Sci.* **62**, 5–13.

Schneider, C.A., Rasband, W.S. and Eliceiri, K.W. (2012) NIH Image to ImageJ: 25 years of image analysis. *Nat. Methods*, **9**, 671–675.

Syvertsen, J.P., Lloyd, J., Mcconchie, C., Kriedemann, P.E. and Farquhar, G.D. (1995) On the relationship between leaf anatomy and CO_2 diffusion through the mesophyll of hypostomatous leaves. *Plant Cell Environ.* **18**, 149–157.

Tenhaken, R. (2014) Cell wall remodeling under abiotic stress. *Front. Plant Sci.* **5**, 771.

Terashima, I., Hanba, Y.T., Tazoe, Y., Vyas, P. and Yano, S. (2006) Irradiance and phenotype: comparative eco-development of sun and shade leaves in relation to photosynthetic CO_2 diffusion. *J. Exp. Bot.* **57**, 343–354.

Terashima, I., Hanba, Y.T., Tholen, D. and Niinemets, Ü. (2011) Leaf functional anatomy in relation to photosynthesis. *Plant Physiol.* **155**, 108–116.

Thain, J.F. (1983) Curvature correction factors in the measurement of cell-surface areas in plant tissues. *J. Exp. Bot.* **34**, 87–94.

Tholen, D., Boom, C., Noguchi, K., Ueda, S., Katase, T. and Terashima, I. (2008) The chloroplast avoidance response decreases internal conductance to CO_2 diffusion in *Arabidopsis thaliana* leaves. *Plant Cell Environ.* **31**, 1688–1700.

Tomás, M., Flexas, J., Copolovici, L. *et al.* (2013) Importance of leaf anatomy in determining mesophyll diffusion conductance to CO_2 across species: quantitative limitations and scaling up by models. *J. Exp. Bot.* **64**, 2269–2281.

Tomás, M., Medrano, H., Brugnoli, E. *et al.* (2014) Variability of mesophyll conductance in grapevine cultivars under water stress conditions in relation to leaf anatomy and water use efficiency. *Aust. J. Grape Wine Res.* **20**, 272–280.

Tosens, T., Niinemets, Ü., Vislap, V., Eichelmann, H. and Castro Díez, P. (2012a) Developmental changes in mesophyll diffusion conductance and photosynthetic capacity under different light and water availabilities in *Populus tremula*: how structure constrains function. *Plant Cell Environ.* **35**, 839–856.

Tosens, T., Niinemets, Ü., Westoby, M. and Wright, I.J. (2012b) Anatomical basis of variation in mesophyll resistance in eastern Australian sclerophylls: news of a long and winding path. *J. Exp. Bot.* **63**, 5105–5119.

Tosens, T., Nishida, K., Gago, J. *et al.* (2016) The photosynthetic capacity in 35 ferns and fern allies: mesophyll CO_2 diffusion as a key trait. *New Phytol.* **209**, 1576–1590.

Valentini, R., Epron, D., Deangelis, P., Matteucci, G. and Dreyer, E. (1995) In-situ estimation of net CO_2 assimilation, photosynthetic electron flow and photorespiration in Turkey oak (*Q. cerris* L) leaves: diurnal cycles under different levels of water supply. *Plant Cell Environ.* **18**, 631–640.

Varone, L., Ribas-Carbó, M., Cardona, C. *et al.* (2012) Stomatal and non-stomatal limitations to photosynthesis in seedlings and saplings of Mediterranean species pre-conditioned and aged in nurseries: Different response to water stress. *Environ. Exp. Bot.* **75**, 235–247.

Veromann-Jürgenson, L.L., Tosens, T., Laanisto, L. and Niinemets, U. (2017) Extremely thick cell walls and low mesophyll conductance: welcome to the world of ancient living!. *J. Exp. Bot.* **68**, 1639–1653.

Weisiger, R. (1998) Impact of extracellular and intracellular diffusion barriers on transport. In *Whole organ approach to cellular metabolism* (Bassingthwaighte, J.B., Goresky, C.A. and Linehan, J.H., eds). New York, NY, US: Springer-Verlag, pp. 389–423.

Weraduwage, S.M., Kim, S.J., Renna, L., Anozie, F.C., Sharkey, T.D. and Brandizzi, F. (2016) Pectin methylesterification impacts the relationship between photosynthesis and plant growth. *Plant Physiol.* **171**, 833–848.

Xiao, Y. and Zhu, X.G. (2017) Components of mesophyll resistance and their environmental responses: a theoretical modelling analysis. *Plant Cell Environ.* **40**, 2729–2742.

Yamori, W., Hikosaka, K. and Way, D.A. (2014) Temperature response of photosynthesis in C3, C4, and CAM plants: temperature acclimation and temperature adaptation. *Photosynth. Res.* **119**, 101–117.

Zablackis, E., Huang, J., Muller, B., Darvill, A.G. and Albersheim, P. (1995) Characterization of the cell-wall polysaccharides of *Arabidopsis thaliana* leaves. *Plant Physiol.* **107**, 1129–1138.

Zhang, T., Tang, H., Vavylonis, D. and Cosgrove, D.J. (2019) Disentangling loosening from softening: insights into primary cell wall structure. *Plant J.* **100**, 1101–1117.

Zhong, R., Cui, D. and Ye, Z.H. (2019) Secondary cell wall biosynthesis. *New Phytol.* **221**, 1703–1723.